EXPERIMENTAL RESPONSE OF A HyFRC BOUNDARY ELEMENT UNDER PURE COMPRESSION

I.D. Williams(1), C.A. Arteta(2), C.P. Ostertag(3)

(1) *PhD student; University of California, Berkeley; ianwilliams@berkeley.edu*
(2) *Assistant Professor, Universidad del Norte, Colombia; carteta@uninorte.edu.co*
(3) *Professor; University of California, Berkeley; ostertag@ce.berkeley.edu*
…

Abstract

Experimental analyses of full-scale reinforced high performance fiber reinforced concrete specimens in compression are scarce in the literature. This paper presents and discusses results of an ongoing study that investigates reinforced concrete prisms representative of boundary elements of special structural walls under compression. Under certain common cross-sectional geometries, such as T- C- and L-shapes, the boundary elements of shear walls are expected to undergo large compressive strains that might trigger flexural-compression failures. This is especially true if the provided transverse reinforcement is not capable of protecting the concrete core against failures under small strain demand increments after the onset of concrete cover spalling. This is explained, in part, because proper confinement is not achievable due to early rebar buckling. Poor experimental performances were observed for some code-compliant prisms, constructed with conventional concrete. This suggested that a practical limit in the longitudinal and transverse reinforcement layouts that can be provided has been reached. Hence, the need for alternative materials arose. The behavior under compressive loading of a high performance Hybrid Fiber Reinforced Concrete (HyFRC) rectangular prism is presented in this paper. Its response is assessed and compared with specimens constructed with conventional concrete without fibers. The HyFRC mix design used in this study utilizes PVA micro-fibers and two types of hooked-end steel macro-fibers, with a total fiber volume percentage of 1.5%. Detailing of transverse reinforcement of the test specimens is compliant with current structural building codes. The specimens were tested under monotonic compression loading until failure. Results indicate that the HyFRC specimens exhibit larger ductility prior to failure as compared to conventional concrete specimens, as well as improved performance of the confined core. In addition, the HyFRC inhibited concrete cover spalling, which retained sufficient lateral tensile capacity to prevent early plastic buckling of the longitudinal rebar. The results also suggest that, given the thin nature of the geometry of the specimens, failure mechanism related to high shear demand in the through-the-thickness direction may arise, also limiting the global compressive strain ductility of the specimen.

Keywords: Hybrid Fiber Reinforced Concrete; Boundary Element; Compression; Buckling; Confinement

1. Introduction

The purpose of this study is to investigate the effect of Hybrid Fiber Reinforced Concrete (HyFRC) on the response of a shear wall boundary element subjected to compressive axial loading. Motivation for this experiment stems from the inspection of shear walls following major earthquakes in Chile (2010) and New Zealand (2011). Failure of multiple walls appeared to initiate in the boundary element region under compression due to crushing of an unconfined core, accompanied by buckling of the longitudinal reinforcing bars. Several studies were performed in the aftermath of this event to investigate the performance of special boundary elements designed according to ACI-318-11. Studies performed by Arteta, et al. [1] and Arteta [2] demonstrated that lateral reinforcement detailing according to current code provisions do not necessarily prevent longitudinal rebar plastic buckling under compressive loading. In light of this study, there is an apparent need to determine alternative methods of restraining the longitudinal reinforcing bars. HyFRC has been studied extensively under flexural and tensile loads, for which it is shown to provide increased ductility and improve post-crack performance [3]. While the behavior of HyFRC in flexure and tension is well understood, fewer studies have been performed to evaluate the potential HyFRC holds for elements subjected to compressive loading. This experiment aims to explore the behavior of HyFRC under compressive loading and determine whether or not the improved tensile capacity of the material is sufficient to restrain longitudinal rebar buckling and improve core confinement.

1.1 Buckling

Buckling of an element under compressive loading is an ever present issue in structural design. Leonhard Euler determined that buckling in slender columns is a form of geometric instability related to the elastic modulus of the material, E, the second moment of area of the cross section, I, and the effective unsupported length of the column, L_e. Using these parameters, Euler derived a simple equation for the elastic buckling load of a slender column, P_e, as shown in Eq. (1).

$$P_e = \frac{\pi^2 EI}{(L_e)^2} \tag{1}$$

Current building codes require lateral reinforcement spacing such that elastic buckling of longitudinal rebar does not occur, thus buckling takes place after yielding of the steel. For example, for columns in special moment frames, ACI-318 [4] restricts transverse reinforcement spacing to six-times the longitudinal bar diameter in zones were plastic demand is expected. This failure mode is referred to as *plastic buckling* and is expected to occur well beyond the elastic limit of strains. The rebar in this case is modeled as a plain steel rod with one end fixed and the other with horizontal and rotational movement restricted, as shown in Fig. 1. Yielding of the steel prior to the elastic buckling load causes a drop in the tangent modulus of elasticity, E_t, introducing additional instability into the system. Onset of inelastic buckling is estimated by plugging the tangent modulus into Euler's buckling equation which results in Eq. (2). Three distinct plastic hinge regions form~~,~~ (shown as the shaded areas of the deformed rod in Fig. 1~~,~~) ~~form~~ at the ends, and in the center of the unbraced length, as the rod begins to buckle ~~as the~~ when approaching critical load, P_c~~, is reached~~. The majority of the deformation concentrates in the plastic hinge regions as buckling progresses.

$$P_c = \frac{\pi^2 E_t I}{(L_e)^2} \tag{2}$$

Comentario [CA1]: I think this definition is problematic because it would mean that bars with a yield plateau (Et=0) cannot strain harden in compression independently of their restriction length.

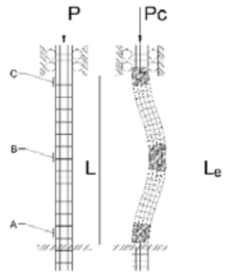

Fig. 1 – Plastic Buckling Column

During axial loading, a perfectly straight reinforcing steel bar in compression would experience a period of zero stiffness in all the material points of the critical section immediately after the yield plateau is reached. According to Eq. (2), at this moment the bar should buckled independently of the length *Le*. In reality, bars in reinforced concrete members are not perfectly straight and the materials points of the critical section reach yielding at different instances. Furthermore, before the onset of plastic buckling some portions of the critical section have already unloaded due to the moment that arises because of the lack of straightness. This in turns causes the materials points to have different elastic moduli preventing the tangent section stiffness E_t from reducing to zero. Fig. 2 presents the results of a plastic buckling simulation for a 7/8-in-diameter rod with 6-in unsupported length. Axial load vs. average strain is plotted on the left axis, and surface strain at the depicted locations along the bar length (see Fig. 1) are shown on the right axis plotted against the average strain over the gage length. Strain on surface at mid-height experience monotonic ~~increased~~ increasing compressive strain as the plastic hinge at the center of the bar curves inward~~,~~; ~~and~~ compressive strain is reduced at the ends of the buckling region as the plastic hinge curves outward. This results in a clear divergence of the surface strains, a behavior which will later be used to evaluate buckling in the longitudinal rebar of the test specimens.

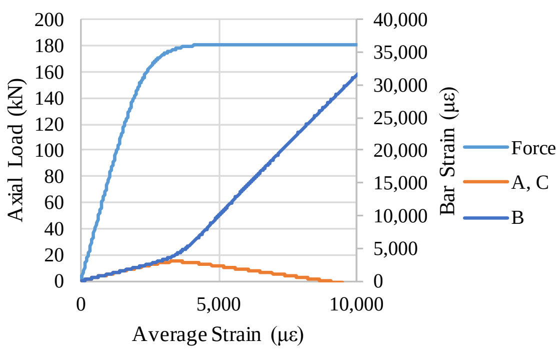

Fig. 2- Buckling bar load and strain behavior

1.2 Mechanism for Delay of Buckling Onset

Properly confined core concrete retains its deformation capacity until the transverse reinforcement fractures and/or the longitudinal bars buckle. Improved tensile performance of HyFRC is demonstrated to be beneficial to multiple aspects of structural performance [3]. Small PVA fibers, 5-mm-long, delay micro-crack initiation, while the larger 30-mm and 60-mm steel fibers arrest macro-cracks and enable multiple cracks to form as opposed to a single, localized, dominant crack [5]. Post-crack tensile strength enhancement and improved ductility due to the inclusion of fibers is apparent in Fig. 3, which shows typical load vs. displacement results for plain concrete and HyFRC flexural beams tested according to ASTM-C1609/C1609M-12 [6].

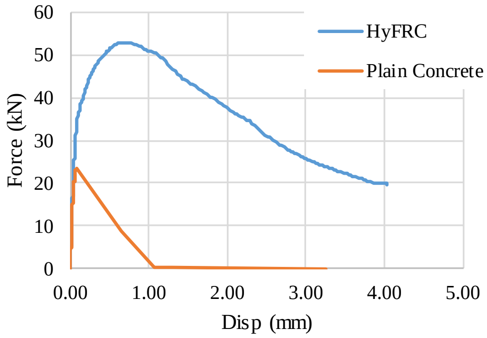

Fig. 3 – Force vs. displacement for plain concrete and HyFRC

While HyFRC has not been extensively studied in compression, early compression tests reveal that HyFRC does not exhibit spalling at high strains, as typically occurs in plain concrete [7,8]. In the case of a typical reinforced concrete compression element with seismic detailing such as a column or a shear wall boundary element, the concrete cover provides distributed lateral support to the longitudinal reinforcement in addition to the horizontal steel reinforcement. This additional support is lost as the cover spalls off, often leading to the initiation of plastic buckling if the bars are not restrained by a tie or the axial stiffness of a hoop leg (e.g. bars restrained by the flexural capacity of a hoop leg). Given the improved tensile characteristics of HyFRC, it is hypothesized that the retained cover in combination with the transverse reinforcement may provide enough support to the longitudinal steel to delay plastic buckling and enable adequate confinement of the core.

2. Test Procedure

The control specimens presented in this study were originally tested as part of a study on the confinement of shear wall boundary elements designed for seismic loading. The cross section of the prismatic specimen is 12 x 36 (305 x 915) with clear height of 72 in. (1830 mm). Specimens are designed according to ACI-318-11 [9] provisions with small variations in the reinforcement detailing (all in accordance with the code) in order to investigate their effects on core confinement. Geometry and reinforcement details for the control specimens C1, C2, and C3 are shown in Fig. 4 and Table 1. Specimen H1 is constructed with HyFRC using the same detailing as control specimen C1. This layout is used as it has the smallest confining ratio (in the through-the-thickness direction) of the three control specimens, which is expected to emphasize the impact of the reinforcing fibers on the global and local response of the wall.

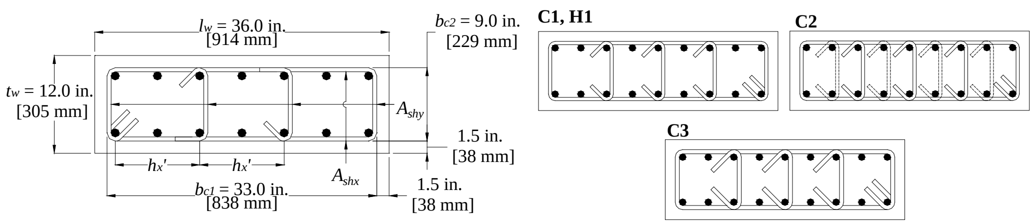

Fig. 4 - Cross section geometry and reinforcement layout of the rectangular prisms

Table 1 – As tested material properties and reinforcement detailing

ID	f'_c ksi (MPa)	f_y ksi (MPa)	f_{yt} ksi (MPa)	d_b in. (mm)	ρ_l %	s in. (mm)	s / d_b	h'_x in. (mm)	d_{bt} in. (mm)	ρ_{tx} %	ρ_{ty} %	$\rho_{t,ACI1}$ %	$\rho_{t,ACI2}$ %
C1	4.4 (30)	67.9 (468)	65.0 (448)	7/8 (22)	2.5	4.0 (102)	4.6	7.7 (196)	1/2 (13)	1.10	0.75	0.91	0.60
C2†	4.4 (30)	76.4 (527)	71.5 (493)	7/8 (22)	2.5	4.0 (102)	4.6 9.2+	7.7 (196)	1/2 (13)	1.10	0.82++	0.84	0.56
C3	4.6 (32)	76.4 (527)	70.3 (485)	7/8 (22)	2.5	4.0 (102)	4.6	7.7 (196)	5/8 (16)	1.70	**1.16**	0.90	0.59
H1	5.0 (34)	69.3 (478)	74.8 (516)	7/8 (22)	2.5	4.0 (102)	4.6	7.7 (196)	1/2 (13)	1.10	0.75	0.97	0.65

†Cross section with ties placed on a checkerboard pattern.

++ Average of two adjacent layers due to the checkerboard pattern used for laying out the ties.

A_{shx}: total cross-sectional area of transverse reinforcement within spacing s, in the long direction of the section.

A_{shy}: total cross-sectional area of transverse reinforcement within spacing s, in the short direction of the section.

b_{c1}: dimension of the long direction of the section core.

b_{c2}: dimension of the short direction of the section core.

h_x': center-to-center horizontal spacing of tied bars in the long direction of the section.

$\rho_{tx} = A_{shx}/(b_{c2} \cdot s)$ and $\rho_{ty} = A_{shy}/(b_{c1} \cdot s)$ are the provided transverse reinforcement ratios in the two principal directions of the cross section.

$\rho_{t,ACI1} = 0.3f'_c / f_{yt} (A_g / A_{ch} - 1)$ and $\rho_{t,ACI2} = 0.09 f'_c / f_{yt}$ are estimated using "as tested" materials properties.

Each prism is tested in uniaxial, monotonic compression until failure. Load is applied using a hydraulically actuated universal testing machine with 4000-kip capacity in compression. The target loading rate for all specimens is 150 kip/minute.

2.1 Expected Response

A simple analytical model is constructed to predict the global load vs. displacement response of the test specimens and is shown in Fig. 5. Load vs. displacement of the section core is predicted using the confined concrete model derived by Mander et al. [10]. The same material model with zero confining stress is used to construct the stress vs. strain curve for the unconfined concrete cover. Longitudinal steel in the section is represented using the Giuffré-Menegotto-Pinto (GMP) steel model with isotropic strain hardening [11].

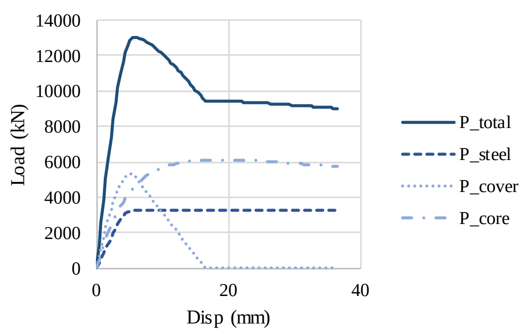

Fig. 5 - Load vs. displacement - expected response

2.2 Instrumentation

Response of the steel reinforcement is monitored through the use of post-yield strain gages oriented parallel the longitudinal bars. All three walls have strain gages attached along the longitudinal bar in the center of the West face of the specimen. This bar is restrained by horizontal ties through the width of the specimen, which are also fitted with strain gages. Specimen H1 has additional strain gages along a longitudinal bar not restrained by ties directly adjacent to the center bar. Concrete response is recorded with the use of strain gages in the core of the wall, on the cover of the wall, and using potentiometric displacement transducers attached to rods which run through the center of the specimen. Out-of-plane displacement is recorded by wire potentiometers (wirepots) oriented normal to the East face of the wall. The instrumentation setup is shown in Fig. 6.

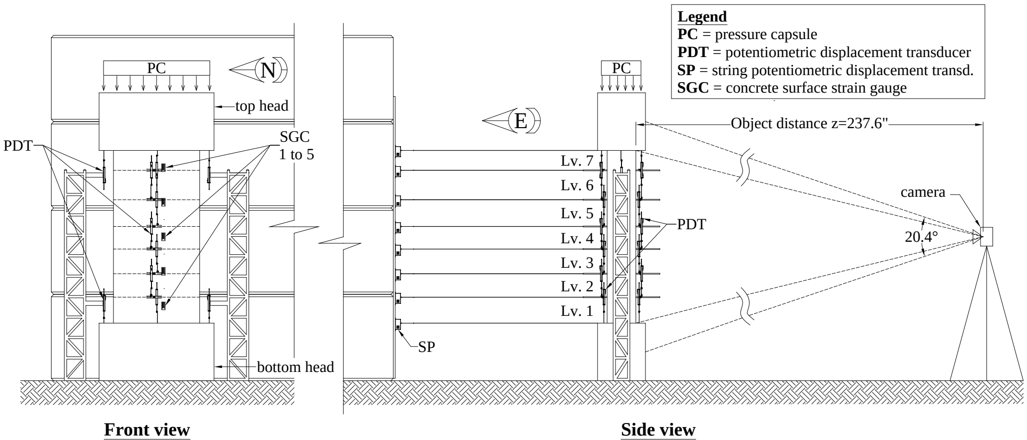

Fig. 6 - Instrumentation setup

3. Materials

3.1 Control Concrete

Control specimens in this study are constructed using concrete ordered from a local mixing plant with nominal 28-day strength of 4.0-ksi [28-MPa]. Actual material compressive strengths for specimens C1, C2, and C3 are contained in Table 1.

3.2 HyFRC

Specimen H1 is constructed using a Hybrid Fiber-Reinforced Concrete mix design which has previously been shown to display deflection-hardening behavior. Compressive and tensile strengths of the HyFRC on the day of testing were f'c=5.0-ksi [34-MPa] and ft=1.1-ksi [7.4-MPa], respectively. Fig. 7a compares normalized stress versus strain curves in compression of the plain concrete of specimen C1 and the HyFRC of specimen H1.

3.3 Steel

Reinforcing bars for all specimens are ASTM-A706/A706M-16 compliant steel. As-tested steel tensile strengths are shown in Table 1. A typical stress vs. strain plot for a steel coupon in tension is shown in Fig. 7b.

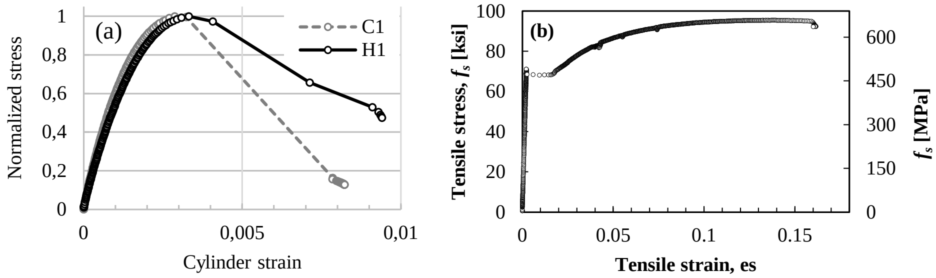

Fig. 7 – (a) Normalized stress versus strain curves comparison of plain concrete (specimen C1) and HyFRC (specimen H1). Note: gage length for strain measurements was 8 in.(200mm). (b) Experimental stress-strain curve for an A706 #7 longitudinal bar.

4. Results

4.1 Global Response

The global load vs. average strain (measured over the 72 in. [1830 mm] of height of the specimen) response for specimens C1, C2, C3, H1, and the predicted response based on material models are shown in Fig. 8. Load values have been normalized to account for different material strengths in each of the control specimens in order to facilitate a fair comparison of the response for each wall. Cover spalling is observed in the three control specimens immediately following the peak load. As large slates of the concrete cover fall from the face of the wall, buckling is observed in the exposed rebar. No such cover spalling is observed in the HyFRC specimen. While specimens C1, C2 and C3 reached their maximum capacity at about 0.003 average axial strain followed by a sudden drop in load carrying capacity, specimen H1 displayed ductile post-peak response up to a strain of 0.008, at which point a sudden load drop occurred. In contrast with the failure mode observed for the regular-concrete specimens, in which cover spalling was accompanied by rebar buckling and loss of concrete core material, the sudden drop in load carrying capacity of specimen H1 is caused by the formation of a shear plane in the through-the-thickness direction of the specimen. Failure modes of control and experimental specimens are shown in Fig. 9.

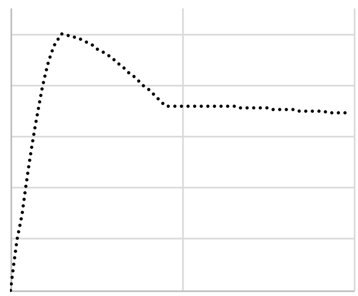

Fig. 8 - Normalized load vs. Avg. strain

Fig. 9 – Failure mode of specimens C1, C2, C3 (left) and H1 (right).

4.2 Local Response

Lateral tie strains and longitudinal rebar strains provide insight into the local performance of the shear wall specimens. Lateral tie strains at key events are plotted along the height of the wall in Fig. 10b and Fig. 11b for specimens C2 and H1, respectively. Strain along wall height for a tied longitudinal reinforcing bar in wall C2 are plotted in Fig. 10c. Strain in both a tied and non-tied longitudinal reinforcing bar in specimen H1 are shown in Fig. 11c and Fig. 11d, respectively.

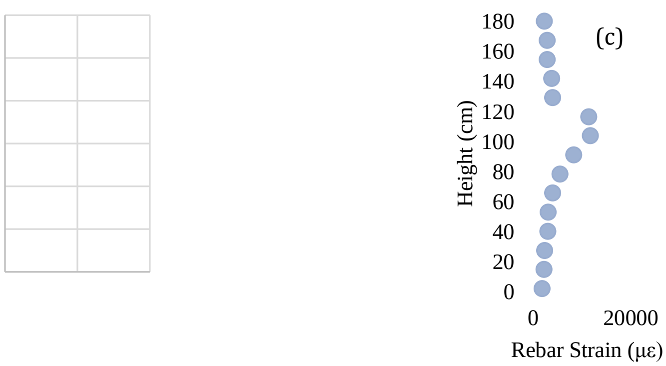

Fig. 10 – Specimen C2: (a) Normalized load vs. avg. strain with locations of key events marked, (b) tie strains along wall height at key events, (c) tied rebar strains along wall height at key events

Fig. 11– Specimen H1: (a) Normalized load vs. avg. strain with locations of key events marked, (b) tie strains along wall height at key events, (c) tied rebar strains along wall height at key events, (d) non-tied rebar strains along wall height at key events

Inspection of the strains in the rebar along the height of each specimen each points to one gage location of greatest strain localization. The gage with greatest localization in specimen C2 is labeled *C2-B*, and the localized gages for a tied and non-tied bar in specimen H1 are labeled *H1-B, tied* and *H1-B, free*, respectively. Fig. 12 shows the strain in *C2-B* along with the strain in the gage below, *C2-A*, and strain in the gage above, *C2-C*, plotted against the average strain over the entire section. Fig. 13a shows the strain in *H1-B, tied* and strain in the gage below, *H1-A, tied*, and the gage above, *H1-C, tied*, plotted against the average strain over the entire section. Fig. 13b shows the strain in *H1-B, free* and strain in the gage below, *H1-A, free*, and the gage above, *H1-C, free*, plotted against the average strain over the entire section. Rebar strains are plotted on the right axis in each of these plots, along with the one-to-one relationship between rebar strain and average section strain. The global response of each specimen is included on the left axis of its respective plot for reference.

Fig. 12 – C2: Axial Force vs. Average Strain (left axis); Rebar Strain vs. Average Strain for selected gages (right axis)

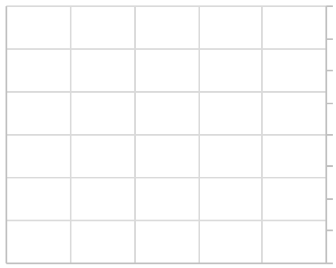

Fig. 13 – (a) H1, tied: Axial Force vs. Average Strain (left axis); Rebar Strain vs. Average Strain for selected gages (right axis); (b) H1, free: Axial Force vs. Average Strain (left axis); Rebar Strain vs. Average Strain for selected gages (right axis);

5. Discussion

5.1 Global Response

A cursory inspection of Fig. 8 is sufficient to show that the HyFRC specimen, H1, exhibits a more ductile failure than control specimen C1 with equivalent lateral reinforcement detailing. Following the initial peak load at a strain of 0.0034, the HyFRC wall recovers capacity and reaches a second peak load at a strain of 0.005. In contrast to this, the capacity of the control specimen declines rapidly following the peak load, losing 8% of its capacity by 0.005 strain, and 29% of its capacity by a strain of 0.008. Capacity of specimen H1 deteriorates slowly following the second peak, falling just 6% between 0.005 and 0.008 strain.

Specimens C2 and C3 show similar response, marked by a sharp decline in strength following the peak load. By a strain of 0.005, specimen C2 has lost 22% of its capacity and C3 has lost 18%. At a strain of 0.008, the capacity of C2 has dropped 56% from its peak, and C3 has dropped 47%.

5.2 Local Response

The poor ductility exhibited by the control specimens is attributed to loss of confinement due to buckling of the longitudinal rebar. Rebar strains in specimen C2, shown in Fig. 12, display similar behavior to the buckling model shown in Fig. 2. This behavior points to buckling in the longitudinal rebar, despite being restrained by lateral reinforcing ties. In contrast to this behavior, the longitudinal rebar strains in Fig. 13a do not diverge in a manner that indicates plastic buckling. The same behavior is seen for a non-tied bar in Fig. 13b, which indicates the stabilizing force on the bar in specimen H1 comes largely from the intact HyFRC cover rather than solely the lateral reinforcing ties.

6. Conclusions

Poor performance of reinforced concrete special structural walls in recent earthquakes and subsequent studies highlights the inability for high aspect ratio compression elements to exhibit ductile response. In light of this observation, there arises a need for improved methods of providing confinement and preventing longitudinal rebar buckling immediately following the peak load. Four rectangular prisms representative of shear wall boundary elements subjected to axial compressive loading are presented in this study. Control specimens C1, C2, and C3 display rapid strength degradation following their first peak load. Comparison of local rebar strains to average section strain for specimens C2 and C3 indicates that this load drop is initiated by plastic buckling in the longitudinal reinforcing bars. Strain localization of lateral ties concurrent with longitudinal bar buckling is determined to reduce the ability of ties to confine the concrete core of the specimen, leading to a sharp drop in capacity.

In contrast to the inadequate response of the control specimens, the prism constructed with HyFRC demonstrated a ~~highly~~ more ductile response. Following the initial peak load, wall H1 managed to recover strength and reach a second, higher peak. This specimen also maintained its capacity, dropping to only 6% below the second peak by a strain of 0.008. At this same strain level, specimen C1 had lost 29% of its capacity, specimen C2 had lost 66% of its capacity, and specimen C3 had lost 47% of its capacity. Furthermore, comparison of local rebar strains to average section strains for specimen H1 indicates that plastic buckling did not occur for a bar restrained by lateral ties nor for one without lateral tie restraint. This demonstrates that the intact HyFRC cover in specimen H1 retains sufficient tensile strength perpendicular to the direction of loading to restrain the longitudinal bars and prevent plastic buckling beyond the compressive strength limit of cover material.

7. References

[1] Arteta C.A., To, D.V. & Moehle, J.P. (2014). Experimental response of boundary elements of code-compliant reinforced concrete shear walls, *Proceedings of the 10th National Conference on Earthquake Engineering, Anchorage, July 21-25 2014*.

[2] Arteta C.A. (2015). Seismic response assessment of thin boundary elements of special concrete shear walls, Doctoral dissertation, Department of Civil and Environmental Engineering, University of California, Berkeley.

[3] Blunt, J., Ostertag, C.P. (2009b). Deflection hardening and workability of hybrid fiber composites, ACI Mat. J., 106:265–272.

[4] ACI-Committee-318. (2014). Building Code Requirements for Structural Concrete and Commentary (ACI 318-14). Farmington Hills, MI: American Concrete Institute.

[5] Blunt, J., Ostertag, C.P. (2009a). A performance based approach for the design of a deflection hardened hybrid Fiber reinforced concrete, ASCE, J. Engrg. Mech., 135:978–986.

[6] ASTM Standard C1609/C1609M-12 (2012). Standard Test Method for Flexural Performance of Fiber-Reinforced Concrete. West Conshohocken, PA, 2012, DOI: 10.1520/C1609_C1609M-12, www.astm.org: ASTM International.

[7] Kumar, P., Jen, G., Trono, W., Panagiotou, M., Ostertag, C.P. (2011). Self Compacting Hybrid Fiber Reinforced Concrete Composites for Bridge Columns. *Technical Report PEER 2011/106*, Pacific Earthquake Engineering Research, Berkeley, USA.

[8] Nguyen, W., Trono, W., Panagiotou, M., Ostertag, C.P. (2014). Seismic Response of a Hybrid Fiber-Reinforced Concrete Bridge Column Detailed for Accelerated Bridge Construction. *Technical Report PEER 2014/19*, Pacific Earthquake Engineering Research, Berkeley, USA.

[9] ACI-Committee-318. (2011). Building Code Requirements for Structural Concrete and Commentary (ACI 318-11). Farmington Hills, MI: American Concrete Institute.

[10] Mander, J. B., Priestley, M. J. N., & Park, R. (1988b). Theoretical Stress-Strain Model for Confined Concrete. Journal of Structural Engineering, 114(8), 1804-1826.

[11] Filippou F.C., Popov, E.P., and Bertero, V.V. (1983). Effects of Bond Deterioration on Hysteretic Behavior of Reinforced Concrete Joints. Report EERC 83/19, Earthquake Engineering Research Center, University of California, Berkeley, 29-35.